ACS Partner Journal

Journal of the American Society for Mass Spectrometry

pubs.acs.org/jasms

Article

Effects of Nano-Electrospray Ionization Emitter Position on Unintentional In-Source Activation of Peptide and Protein Ions

Samantha O. Shepherd, Austin W. Green, Elizabeth S. Resendiz, Kenneth R. Newton, Ruwan T. Kurulugama, and James S. Prell*

Cite This: *J. Am. Soc. Mass Spectrom.* 2024, 35, 498−507

Read Online

ACCESS | Metrics & More | Article Recommendations | Supporting Information

ABSTRACT: Native ion mobility−mass spectrometry (IM-MS) typically introduces protein ions into the gas phase through nano-electrospray ionization (nESI). Many nESI setups have mobile stages for tuning the ion signal and extent of co-solute and salt adduction. However, tuning the position of the emitter capillary in nESI can have unintended downstream consequences for collision-induced unfolding or collision-induced dissociation (CIU/D) experiments. Here, we show that relatively small variations in the nESI emitter position can shift the midpoint (commonly called the "CID50" or "CIU50") potential of CID breakdown curves and CIU transitions by as much as 8 V on commercial instruments. A spatial "map" of the shift in CID50 for the loss of heme from holomyoglobin onto the emitter position on a Waters Synapt G2-S*i* mass spectrometer shows that emitter positions closer to the instrument inlet can result in significantly greater in-source activation, whereas different effects are found on an Agilent 6545XT instrument for the ions studied. A similar effect is observed for CID of the singly protonated leucine enkephalin peptide and Shiga toxin 1 subunit B homopentamer on the Waters Synapt G2-S*i* instrument. In-source activation effects on a Waters Synapt G2-S*i* are also investigated by examining the RMSD between CIU fingerprints acquired at different emitter positions and the shifts in CIU50 for structural transitions of bovine serum albumin and NIST monoclonal antibody.

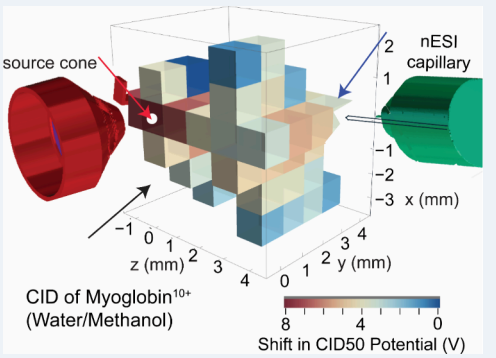

KEYWORDS: *electrospray ionization, activation, native mass spectrometry, collision-induced dissociation*

INTRODUCTION

Native mass spectrometry (and its variant coupled to ion mobility spectrometry, IM-MS) can be a powerful tool to probe protein structures and interactions. Nano-electrospray ionization (nESI) is widely used for native IM-MS because it can transfer kinetically trapped native-like structures to the gas phase for structure analysis. nESI has been shown to be capable of retaining secondary, tertiary, and quaternary structure in many protein complexes both experimentally[1−4] and computationally.[5−7] By deliberately adding internal energy to native-like ions in the gas phase, collision-induced unfolding (CIU) and/or dissociation (CID) can be used to identify differences in biomolecular structures, augmenting the capabilities of native IM-MS.[8−12] These structural differences range from being relatively large, such as those in high-order structure or ligand binding sites,[13−17] to much more subtle, such as those due to differences in proteins with nearly identical collision cross section distributions in the absence of deliberate activation.[18] Structural information determined by native IM-MS often agrees very well with results from more traditional biophysical and biochemical techniques.[3,4,11,15,16,19−29]

Although nESI can kinetically trap biomolecular complexes in native-like structures, it is also known that the chemical and physical properties of the nESI droplet are dynamic.[24,30−35] For example, even with the use of volatile buffer salts such as ammonium acetate, the effective pH of droplets can change by as much as 2 pH units as the droplets evaporate,[36,37] and over time, nESI may acidify neutral ammonium acetate solutions in positive ion mode nESI.[38] Other examples of protein disruption in nESI include redox reactions associated with nESI,[39,40] intrinsic native electron capture dissociation (ECD),[41] annealing of the nascent analyte ion,[3,49] electrothermal supercharging,[42] and nozzle−skimmer dissociation[43−45] (a type of in-source CID).

Collisional activation (i.e., nozzle−skimmer dissociation) has long been used to deliberately activate and fragment nascent biomolecular ions in MS as they enter the instrument, but collisional activation (CID and CIU) inside the instrument is more commonly used in modern instruments due to more precise control of energy deposition and the ability to first

Received: October 20, 2023
Revised: January 26, 2024
Accepted: January 31, 2024
Published: February 20, 2024

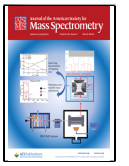

isolate ions of interest.[1] In CIU/D, modern instruments typically use an adjustable electric potential (the "injection potential") to accelerate the analyte ion into a region filled with a buffer gas. Collisions between the analyte ion and the gas heat the analyte, causing dissociation and/or unfolding. The fraction of the remaining precursor ion can be plotted as a function of injection potential to produce a breakdown curve. A common metric to compare breakdown curves generated by these methods are CID50 and CIU50 values, i.e., the injection potential at which 50% of the precursor ion has undergone a measurable dissociation or change in the collision cross section, respectively.[46−48] Because collision gas and pressures, collision cell design, and other properties can differ greatly between instruments and may be user-controlled, CIU50 and CID50 values can be challenging to compare between instruments or under experimental conditions. For example, within a single instrument, activation early on in the ion path, e.g., in the StepWave of a Waters Synapt G2-S*i* instrument, can shift breakdown curves and CIU fingerprints along the injection potential axis.[3,49] This shift can be "additive" in the sense that CIU50 values for successive structural transitions are all shifted to higher voltages by approximately the same amount on this instrument, but it is not generally known whether this is the case for other instruments, where ions may experience very different buffer gas pressure profiles and electric fields.

A handful of previous studies have shown that the position and orientation of the emitter in conventional electrospray ionization and nESI can affect the observed mass spectrum and in-source activation of protein−ligand complexes,[35,50,51] and other studies have investigated the internal energy distribution of ions in ESI.[33,52−56] These studies have shown that the emitter position, emitter orientation, and electrospray potential can individually help desolvate and desalt ions and increase mass accuracy, but some combinations of them can lead to dissociation. These studies have also demonstrated that greater desalting can occur when there are longer distances between the emitter opening and the instrument inlet.

Control and reproducibility of ion charge state distributions[57] and structures using nESI can be a hurdle to obtaining highly consistent CIU and CID data, both over time and between laboratories. nESI emitters, which can vary in both material and physical dimensions, are often pulled to different opening diameters by different methods in different laboratories,[58−60] likely resulting in different initial nESI droplet sizes. Laboratories often further optimize the source temperature and emitter position to optimize the signal strength and reduce the degree of unwanted co-solute or salt adduction, though the precise position of the emitter is rarely reported in publications and may vary from user to user or even spectrum to spectrum. A small number of reports in the literature have examined the variability in CIU/D data and explored design principles to increase reproducibility. Loo and co-workers attributed variation in mass spectra and ion behavior between users without a clear explanation to different users having a different "touch" for ESI.[35] They reported that each user, even on the same day, observed differences in mass spectra of protein and protein complex analytes generated from ESI. In contrast, a collaborative effort between three laboratories showed that an "in-source CIU" modification for Agilent Technologies 6560C IM-MS instruments can reduce CIU fingerprint RMSD (root-mean-square deviation) values for the same analyte between source hardware to less than 5%.[61]

Here, the effects of the nESI emitter position on in-source ion activation in CID and CIU experiments are systematically studied on two different commercial instruments (a Waters Synapt G2-S*i* quadrupole−IM−time-of-flight (Q-IM-TOF) instrument and an Agilent 6545XT Q-TOF instrument) for several protein and peptide ions. Based on these results, strategies are provided for use in nESI-(IM)-MS experiments to minimize unintentional in-source activation and increase reproducibility.

METHODS

All peptide and protein samples were obtained from Sigma-Aldrich (St. Louis, Missouri, U.S.A.) as lyophilized proteins and used without further purification. Equine heart myoglobin (SKU: M1882), leucine enkephalin acetate salt (SKU: L9133), bovine serum albumin (BSA, SKU: 05470), Shiga toxin 1 subunit B (SKU: SML0562), and NIST IgG1κ monoclonal antibody (NIST mAb, SKU: 8671) were reconstituted in water and buffer swapped using Micro Bio-Spin 6 columns (Bio-Rad, Hercules, California, U.S.A.) into 200 mM ammonium acetate solution (pH = 7.4) to generate native protein solutions. Partially denatured myoglobin solution, as described elsewhere,[51] was also prepared to yield a myoglobin sample with a single dominant CID loss channel. For this sample, reconstituted holomyoglobin was buffer swapped into 18 MΩ·cm water and diluted with methanol (Thermo Scientific, Waltham, Massachusetts, U.S.A.) to yield an 80/20 vol/vol water/methanol solution. All final sample concentrations ranged from 5 to 15 μM with the exception of a high-concentration native myoglobin sample prepared as 35 μM. The nESI source on both instruments was operated in positive ion mode under static nESI conditions using 1.0/0.78 mm o.d./i.d. (outer diameter/inner diameter) borosilicate glass nESI emitters pulled to ∼2 μm i.d. openings using a P97 Flaming-Brown micropipette puller (Sutter Instrument, Novato, California, U.S.A.) without further modification. nESI was initiated by applying a 0.9−1.5 kV potential to a platinum wire inserted into the solution inside the emitter without the use of an external syringe pump. Throughout the manuscript, the term "close" refers to the emitter position in which the tip of the emitter is as close to the entrance of the instrument as possible without breaking the tip of the emitter on the instrument inlet cone (an *xyz* position of 0 ± 0.2, 0.5 ± 0.5, 0 ± 1 mm relative to the center of the inlet, where *x*, *y*, and *z* represent the vertical [above/below the center of the inlet cone], horizontal along inlet axis, and horizontal perpendicular to inlet axis distances relative to the inlet, respectively). "Far" positions varied. A complete description of all positions used is included in Table S1.

To assess the variability in nESI emitter dimensions, a field-emission, variable-pressure scanning electron microscope (Thermo Fisher Apreo 2S Lo, Thermo Scientific, Massachusetts, U.S.A.) was used. The inner diameter of the pulled emitter openings overall was 2.2 ± 0.6 μm, and the distance from the onset of the taper at the end of the emitter to the emitter opening was 3.3 ± 0.1 mm. Further information on emitter reproducibility and settings is included in the Supporting Information (SI) (see Appendix S1 and Figure S1).

All (IM-)MS data were analyzed using UniDec,[62] Python, and CIUSuite 2 (using settings listed in Table S2).[63] For CIU experiments, RMSD "average of pairwise root-mean-square

https://doi.org/10.1021/jasms.3c00371
J. Am. Soc. Mass Spectrom. 2024, 35, 498−507

deviation" ($RMSD_{AofP}$) is used to refer to the average of two or more experiment-to-experiment pairwise RMSD values, and $RMSD_{PofA}$ is used to refer to the pairwise RMSD of two averaged CIU fingerprints. Further discussion of the differences between these metrics is included in the SI (Appendix S2). Data for CIU experiments were collected in quintuplicate at each position with 3 of the 5 trials collected using the self-same emitter without moving it.

RESULTS AND DISCUSSION

Choice of Samples. CID can be used to fragment covalent bonds in both peptides (e.g., in bottom-up and middle-down proteomics) and proteins (e.g., in top-down proteomics) as well as noncovalent bonds in native MS. In order to survey the effects of the nESI emitter position in both CID and CIU, we used the common MS standard peptide leucine enkephalin (amino acid sequence YGGFL)[66] and the proteins equine holomyoglobin (which dissociates by loss of a noncovalently bound heme ligand), Shiga toxin 1 subunit B pentamer (as an example of a homooligomer), bovine serum albumin (BSA, which has multiple accessible CIU transitions), and NIST humanized IgG1κ monoclonal antibody (NIST mAb, as a representative of this class of mAb, which is of major current interest in CIU applications).[18] Holomyoglobin, notably, is known to exhibit two competitive CID channels (loss of positively charged heme and loss of neutral heme)[39] when prepared by nESI from aqueous ammonium acetate, whereas it dissociates almost exclusively by loss of charged heme when prepared by ESI from 80/20 water/methanol solution. The latter behavior is attributed to partial denaturation of the protein in the water/methanol solution, consistent with its slightly shifted charge state distribution in the positive ion mode (see Figure 1). However, the extent of denaturation is not sufficient to lose the heme in solution, and the precise blackbody infrared radiative dissociation (BIRD) values obtained for the partially denatured ions in studies by the William group indicate that the ions' structures are still relatively homogeneous.[64] Furthermore, it is known that the oxidation state of native holomyoglobin and the relative prevalence of the neutral versus charged heme loss channels upon CID are correlated.[39] Loss of heme^0 from holomyoglobin upon CID has been associated with precursor holomyoglobin containing Fe(II), and loss of heme^{1+} is associated with precursor holomyoglobin containing Fe(III). The latter oxidation state can result from oxidation of the nESI solution after many minutes of continuous spray, but it has been shown that other heme-containing proteins can undergo intrinsic native ECD at high concentrations to produce monomers containing Fe(III).[41]

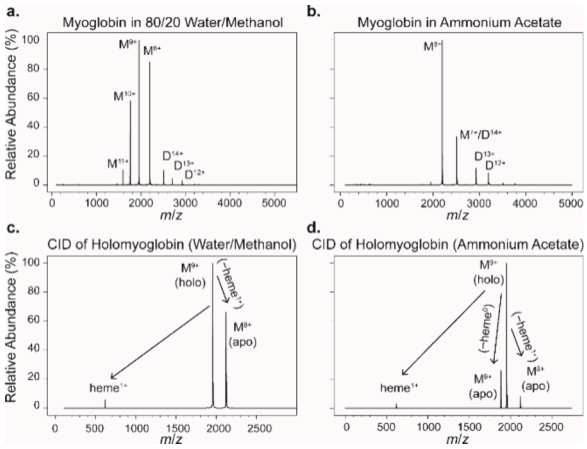

Figure 1. Mass spectra for myoglobin ions from (a) 80/20 water/methanol and (b) aqueous ammonium acetate. The primary dissociation channels for each solution condition are shown in (c) water/methanol (loss of heme^{1+}) and (d) ammonium acetate (competitive loss of heme^0 and heme^{1+}).

Figure 1 shows example mass spectra for CID of holomyoglobin ions prepared by nESI from 80/20 water/methanol (partially denatured, Figure 1a) and from neutral 100 mM aqueous ammonium acetate (native-like, Figure 1b). CID of holomyoglobin from water/methanol is strongly dominated by a single dissociation channel via the loss of heme^{1+} (Figure 1c), while CID of holomyoglobin from ammonium acetate exhibits both this loss channel and the loss of heme^0 (Figure 1d). The single CID channel for holomyoglobin from the 80/20 water/methanol solution facilitated the determination of CID50 values when using different nESI emitter positions in many of the experiments described below.

Assessment of Protein CIU and CID Repeatability Using a Single nESI Emitter and Fixed Emitter Position. In both CID and CIU experiments on native-like proteins, it is often necessary to repeat measurements with different nESI emitters, and, as described in the Introduction, the emitter position is often tuned to some extent to maximize the signal and remove salt adducts. To assess the contributions of using different emitters and emitter positions to variability in CID and CIU, it was necessary to first characterize the variability associated with the case in which a single emitter is used without changing its position. For CIU, we used metrics commonly used in comparing CIU fingerprints. CIU fingerprints are often acquired in triplicate, and the triplicate-average root-mean-square deviation (RMSD) between each pair of maximum-intensity-normalized fingerprints is reported as a percentage ("average pairwise RMSD", hereafter $RMSD_{AofP}$) to assess variability. Here, CIU fingerprints of NIST mAb^{25+} were acquired in triplicate (Figure 2a–c) using a single nESI emitter in a fixed position and Traveling Wave Ion Mobility Spectrometry (TWIMS) instrumentation settings of 650 m/s and 30 V. When averaged (Figure 2d), these fingerprints showed a very low $RMSD_{AofP}$ (1.19%, Figure 2e,f).

A similar set of CIU experiments was performed for BSA^{16+}, and a very low $RMSD_{AofP}$ (0.98%, data not shown) was measured. Additional single-emitter $RMSD_{AofP}$ values for NIST mAb^{22-26+} and BSA^{14-16+}, averaged over all charge states, are shown in Figure 2f, alongside values for the most abundant charge states of each protein. These results show that CIU fingerprints collected sequentially using a single emitter can be highly repeatable ($RMSD_{AofP} \sim 4\%$), especially for high-abundance charge states ($RMSD_{AofP} \sim 3\%$).

Reproducibility of CID and CIU Using Fixed versus Uncontrolled nESI Emitter Position. CID of singly protonated leucine enkephalin peptide (555 Da) generated by nESI from a solution of aqueous ammonium acetate (pH = 7) was performed on the Synapt G2-S*i* instrument using injection potentials between 5 and 35 V. CID of holomyoglobin^{7-10+} ions (17 549 Da) generated by nESI from a solution of 80/20 water/methanol (v/v) was performed with injection potentials between 5 and 65 V. Figure 3 shows CID breakdown curves for leucine enkephalin (Figures 3a,e)

https://doi.org/10.1021/jasms.3c00371
J. Am. Soc. Mass Spectrom. 2024, 35, 498−507

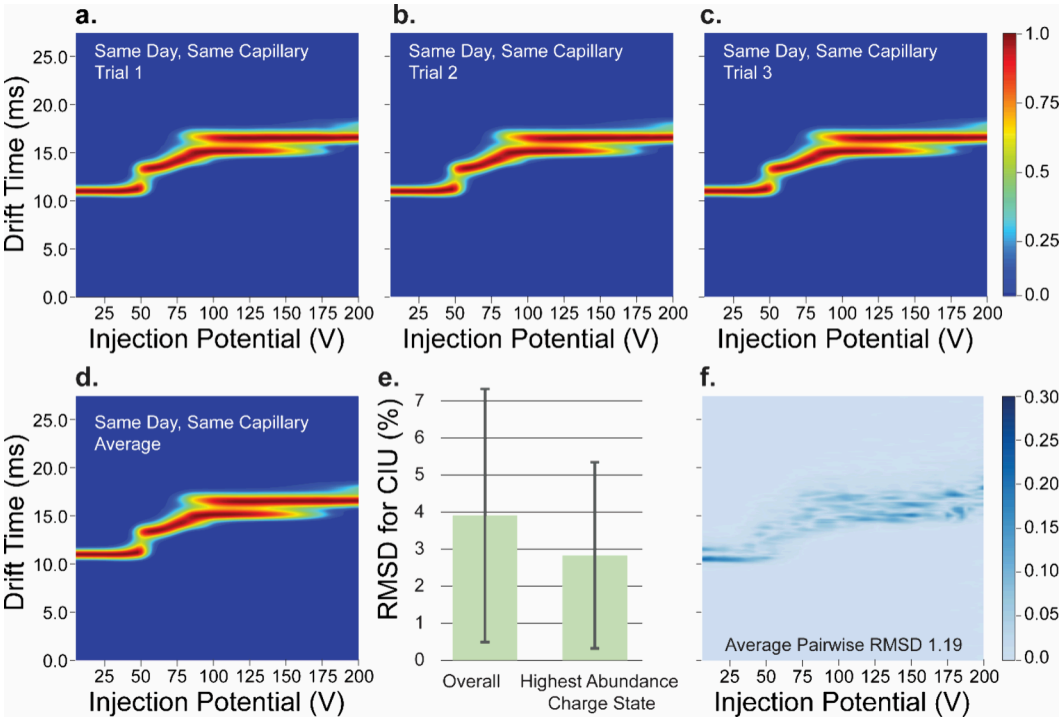

Figure 2. (a–c) CIU fingerprints of NIST mAb^{25+} collected in triplicate using a single nESI emitter in a fixed position. The average of these fingerprints is shown in (d). (e) Average (green bar) and single standard deviation (error bars) in pairwise RMSD of CIU fingerprints for all native charge states of NIST mAb (22–26+) and BSA (12–14+) and for only the most abundant charge state (NIST mAb^{25+} and BSA^{16+}). (f) Average CIU difference plot for the fingerprints shown in (a–c) for NIST mAb^{25+}.

and holomyoglobin$^{9,10+}$ in water/methanol (Figures 3b,c,f,g) in uncontrolled (Figures 3a–c) and fixed (Figures 3e–g) emitter positions across multiple days.

In the uncontrolled nESI emitter position experiments, the position of the nESI emitter was coarsely tuned by a single user for a high precursor signal while minimizing sodium adduction. The CID50 for all three ions (leucine enkephalin and holomyoglobin$^{9,10+}$) had a roughly inverse correlation with the signal strength. (Figure S2 shows example data for holomyoglobin^{9+} from 80/20 water/methanol solution.) That is, a higher precursor signal corresponded to greater in-source activation (lower CID50), and positions with a lower signal corresponded to less in-source activation (higher CID50; see Figure S2). In contrast, controlling the emitter position by using identical nESI stage micrometer settings between days and emitters significantly reduced the variability of the replicate-average CID50 for these ions (Figure 3i). The standard deviation in the CID50 for the fixed emitter position experiments was lower by a factor of ∼3–6 for all three analytes as compared to that for the uncontrolled emitter experiments. Thus, as for CIU (see above), repeatability in CID experiments can be very high when using a fixed emitter position. These results show that controlling the emitter position can improve the reproducibility of CID experiments. In principle, use of a controlled emitter position can thus increase confidence in interpreting CID50 differences between proteins as structural or stability differences, especially if the emitter position is recorded and reported alongside other experimental parameters.

An analogous set of experiments was used to assess the effects of the nESI emitter position on CIU of BSA^{15+} on a Waters Synapt G2-*Si* instrument using injection potentials from 5 to 200 V. RMSD values were calculated for uncontrolled emitter positions across multiple days (Figure 3d) and for a fixed emitter position using multiple capillaries (three on the same day; Figure 3h). For BSA^{15+}, the $RMSD_{AofP}$ for the uncontrolled emitter position experiments (27.91%) was far higher than the accepted standard for reproducibility (<5%).[61] In sharp contrast, the $RMSD_{AofP}$ for the fixed emitter position triplicate collected on the same day was 4.30%, which falls within this standard and is clearly higher than that obtained for the triplicate by using a single emitter (see above). An effect of similar magnitude of exchanging emitters was observed for all charge states of BSA (14–16+) and NIST mAb (22–26+) that were investigated. The overall $RMSD_{AofP}$ for both proteins was determined to be 6 ± 3% across all charge states and 4 ± 2% for the most abundant charge states. Because variation in CIU fingerprints acquired using different emitters in the same position can be larger than that using a single emitter, it is therefore recommended to use multiple emitters to accurately survey the CIU variability for a fixed emitter position. In contrast to the CID experiments described above, use of an uncontrolled emitter position to optimize for high signal and low salt adduction in CIU resulted in a similar amount of variation (as measured by $RMSD_{AofP}$) as did exchanging emitters in a fixed position (Figure 3j).

Taken together, the above results show that controlling the nESI emitter position can significantly reduce variability in CID50 and reduce CIU RMSD. Noting and reporting the emitter position (e.g., the nESI stage micrometer positions and stand-off of the nESI emitter tip from the stage) can thus facilitate reproducibility between laboratories and improve traceability as well as provide crucial information for literature meta-analysis.

Spatial Map of Extent of In-Source Activation Due to Emitter Position in CID Experiments. Motivated by the

https://doi.org/10.1021/jasms.3c00371
J. Am. Soc. Mass Spectrom. 2024, 35, 498–507

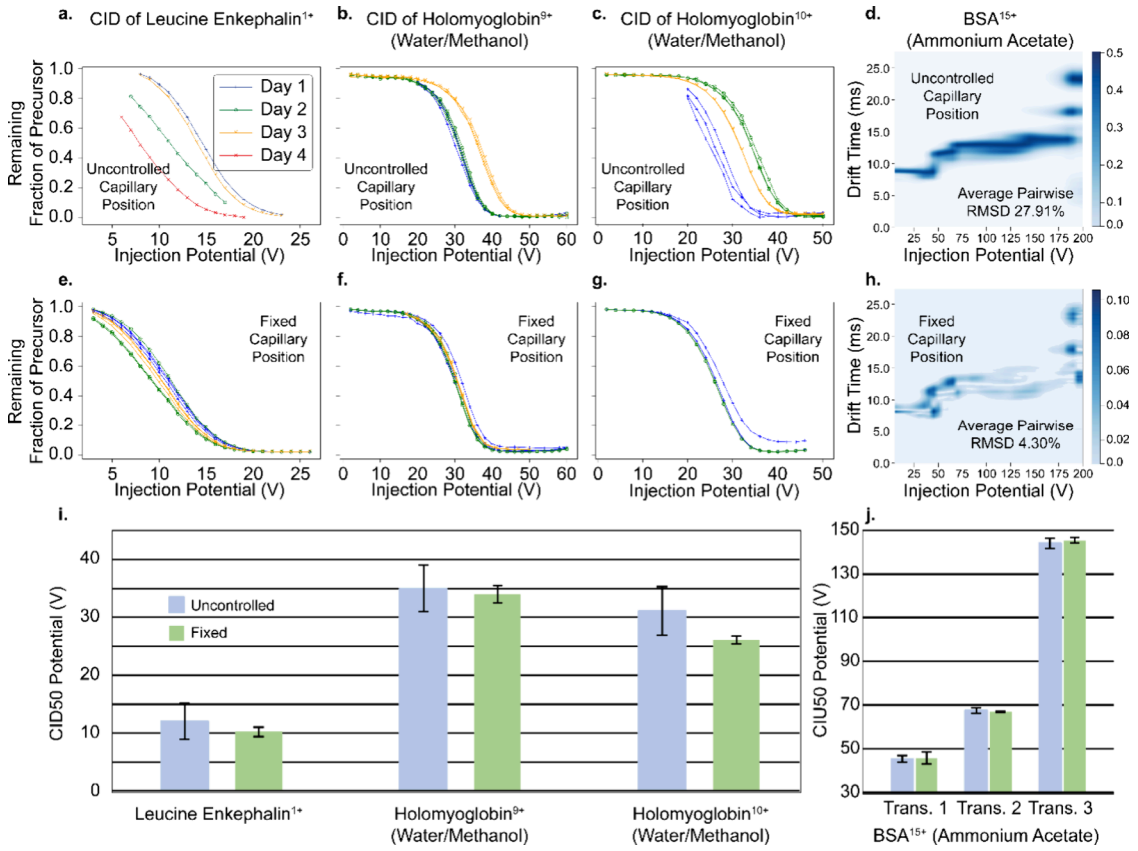

Figure 3. (a–c, e–g) CID breakdown curves and (d, h) CIU fingerprint differences in (a–d) uncontrolled and (e–h) fixed nESI emitter positions on a Waters Synapt G2-*Si* instrument for (a, e) leucine enkephalin, (b, f) holomyoglobin^{9+}, (c, g) holomyoglobin^{10+}, and (d, h) BSA^{15+}. Statistics for CID50 are summarized in (i), with error bars representing the standard deviation of the CID50 value across all trials. Statistics for CIU50 of BSA^{15+} are summarized in (j), with error bars representing the standard deviation in CIU50 value across three trials.

above-described influence of the nESI emitter position on the variability of CID and CIU data, we investigated whether there was a spatial mapping of this effect onto the emitter position and to what extent this effect may vary between different instruments and analytes. Figure 4a shows a spatial map of CID50 onto the nESI emitter position for partially denatured holomyoglobin^{9+} on the Waters Synapt G2-*Si* instrument. (An analogous map for holomyoglobin^{10+} is shown in Figure S3.) Representative CID breakdown curves in three emitter positions ("far", "below", and "close"; see Figure 4b) show shifts of the entire breakdown curve along the injection potential axis. On the spatial map, emitter positions for which the CID50 is shifted to lower values indicate greater in-source activation for this ion. As can be seen in the spatial map, emitter positions that cause higher in-source activation are located roughly along the inlet axis out to ~3 mm in front of the inlet and then follow a roughly 90° turn toward the axis of the emitter holder. The most activating of these are the positions closest to the inlet. Other, more "peripheral" emitter positions cause less in-source activation.

Based on this map, CID was also performed at "high" and "low" activation positions for singly protonated leucine enkephalin (Figure S4a–d; representative mass spectra are shown in Figure S5), native Shiga toxin 1 subunit B pentamer (Figure S4e), and native holomyoglobin^{9+} (Figure 4c) to determine whether a similar spatial pattern holds for other analytes. Differences of ~3 and 4 V were observed for leucine enkephalin and Shiga toxin 1 subunit B pentamer, respectively, with greater in-source activation at the emitter position close

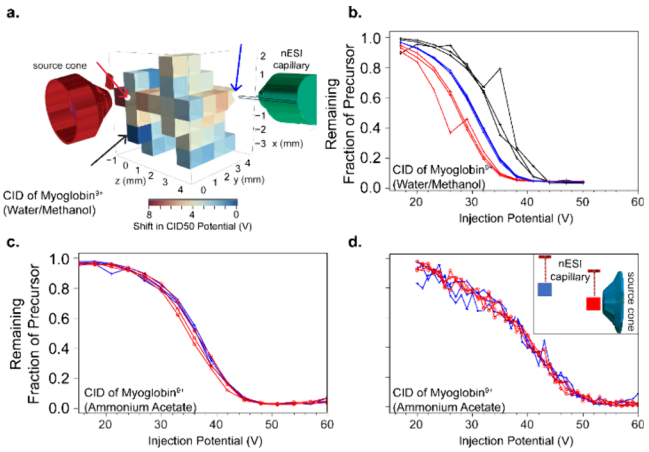

Figure 4. (a) A map of the effect of position on CID50 of holomyoglobin in water/methanol on a Waters Synapt G2-*Si* instrument. Blue cubes show the highest CID50 potential required, while red cubes show the lowest. (b) CID breakdown curves of holomyoglobin water/methanol at the "close" (red; 0, 0.5, 0.5 mm), "far" (blue; 0, 3, 5 mm), and "below" (black; − 3, 1, 1 mm) positions. These positions are shown with arrows in (a). (c) CID breakdown curves of holomyoglobin in ammonium acetate on the Waters Synapt G2-*Si* at the close (red) and far (blue) positions. (d) CID breakdown curves of holomyoglobin in ammonium acetate on the Agilent 6545XT Q-TOF mass spectrometer at "close" (red; 0.5, 2 mm) and "far" (blue; 2, 5 mm) positions. See the Methods section for an explanation of emitter position coordinates.

https://doi.org/10.1021/jasms.3c00371
J. Am. Soc. Mass Spectrom. 2024, 35, 498−507

to the inlet (Figure S4). A smaller difference of 0.8 V was observed for native myoglobin^{9+} (Figure 4c). Results for all three of these analytes qualitatively agree with the map for partially denatured holomyoglobin^{9+}.

To ascertain whether a similar spatial dependence applies to a different instrument source, the influence of position on an Agilent 6545XT Q-TOF mass spectrometer was studied using native myoglobin and leucine enkephalin with the nESI emitter located close (~1−3 mm) and far (~4−7 mm) from the instrument inlet. On this instrument, no significant difference in CID50 was observed for leucine enkephalin (Figure S6) or moderate-concentration (8 μM) myoglobin (Figure 4d) between the two emitter positions. However, when using a high-concentration (35 μM) native myoglobin sample on the Agilent 6545XT mass spectrometer (located on the axis with the instrument inlet on the other side of the nESI emitter), use of the far emitter position resulted in greater competition between the heme$^{0/1+}$ loss channels upon CID. Almost all CID occurred by the loss of heme^{1+} in the close position (see Figure S7). These results illustrate that effects of the nESI emitter position on CID can be instrument-dependent. While for the Waters Synapt G2-S*i* instrument, measurably different amounts of in-source activation occurred at close versus far positions for all three analytes, only small (average of <0.5 V) differences were observed for the Agilent 6545XT instrument for a similar distance between emitter positions for two of the three tested analytes.

Intriguingly, a large difference in the CID branching ratio (heme^{0} versus heme^{1+} loss channels) on the 6545XT was observed for high- (but not low-) concentration holomyoglobin solutions with a large (~7 V) concomitant shift in CID50 (see Figure S7). This effect may be due to electrochemical oxidation in solution[39] due to the higher electric fields present in the closer emitter position, or it may be due to redox activity within weakly bound dimers at the higher concentration. Brandner et al. recently reported the "intrinsic native electron capture dissociation" of (heme-containing) cytochrome c that only occurs at high (≥37.5 μM) concentrations and requires no deliberate collisional activation.[41] They attributed this to intermonomer electron transfer in cytochrome c dimers somewhere within the instrument source region. Here, it appears that emitter-position-dependent activation differences on the Agilent 6545XT are insufficient to significantly affect the CID of either leucine enkephalin or native holomyoglobin monomers but are sufficient to cause observable differences for holomyoglobin at high concentrations. The CID50 values for these experiments are summarized in Figure S8.

The Waters Synapt G2-S*i* instrument and the Agilent 6545XT mass spectrometer (see photographs and schematics in Figure S9) have significantly different source designs, which may explain the observed differences in nESI emitter-position-dependent activation. One major difference is that inside the Synapt G2-S*i* source, ions travel through a relatively high-conductance (~15 mm diameter) ion guide into the "StepWave", whereas for the Agilent 6545XT, they pass through a narrow (0.60 mm in diameter, 18 cm long) inlet capillary followed by a supersonic expansion into the capillary-skimmer interface. The nESI potential needed for stable spray across all emitter positions on the Agilent 6545XT (1.2−1.5 kV) was slightly higher than that used on the Waters Synapt G2-S*i* (0.9−1.3 kV). Nitrogen drying gas is used in the Agilent 6545XT source, whereas no drying gas was used in these Waters Synapt G2-S*i* experiments. The range of emitter-to-inlet distances and the source temperatures (24−31 °C) used in the two sources are similar. Together, these design differences suggest that the above-described differences in CID behavior arise primarily from differences in the sharpness of the transition from atmospheric to low pressure and the amount of time that ions spend beyond the source inlet at relatively high pressure in the two instruments.

Variation of Protein CIU Fingerprints at Fixed Emitter Positions As Measured Using RMSD. Above, it was shown that using a fixed emitter position with a single emitter can result in very low variability in CID50, CIU50, and CIU RMSD between replicates. To determine whether different emitter positions also cause different measurable in-source activation in CIU experiments, we first investigated whether RMSD for replicates using a single emitter at a fixed position varied with the emitter position. Generating CIU fingerprints with a low RMSD is a widely accepted criterion for high reproducibility/repeatability and is necessary to confidently distinguish structures of ions based on differences in their CIU fingerprints.

RMSD values for CIU fingerprints acquired at different emitter positions were calculated to assess whether these data met the <5% acceptance criterion and to quantify their variability. These data were collected in a same-day quintuplicate using BSA and NIST mAb (mass spectra are shown in Figures S10 and S11), as described in the Methods section. BSA fingerprints were collected in this way on 3 separate days, and NIST mAb fingerprints were collected on a single day (representative data shown in Figures S12−S14). The results in this section for BSA are reported as the average across those 3 days. Figure 5 summarizes the measured effects of different capillaries at positions close to and far from the instrument inlet. The nESI emitter position effects on the repeatability (using a single emitter) and reproducibility (between different emitters) of CIU fingerprint replicates

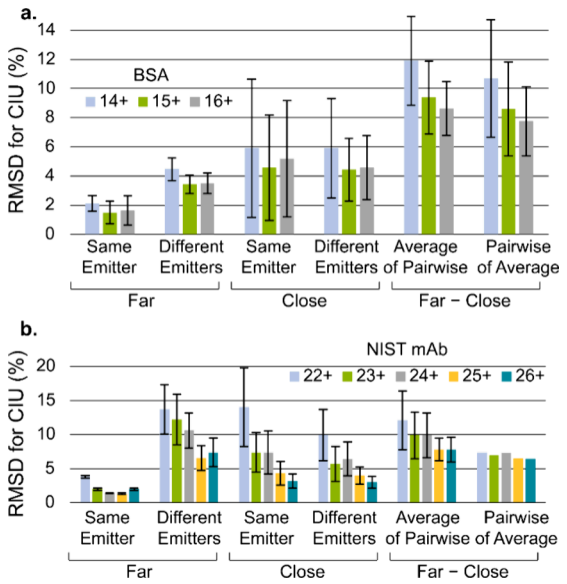

Figure 5. Statistics for RMSD of (a) quintuplicates of BSA collected on three separate days and (b) quintuplicates of NIST mAb collected on a single day. In (a), colored bars represent the average, and error bars represent the combination of triplicate and day-to-day variation. In (b), colored bars represent the average, and error bars represent the triplicate variation.

https://doi.org/10.1021/jasms.3c00371
J. Am. Soc. Mass Spectrom. 2024, 35, 498−507

were measured by the RMSD values calculated in CIUSuite 2 for BSA (Figure 5a) and NIST mAb (Figure 5b). The average RMSD across 3 days and all 5 fixed-position replicates for BSA was less than 6% (and less than 5% for the highly abundant 15 and 16+ charge states; see Figure 5a). The average RMSD for NIST mAb exceeded 10% for two of the low-abundance native charge states (22 and 23+) under some conditions, which is outside the acceptance criterion established by Ruotolo and co-workers. However, for high-abundance charge states (25 and 26+) at both close and far positions, it was less than 7% overall, and for most fingerprints, it was less than 5% (Figure 5b).

Loo and co-workers observed that results from native MS experiments can to some extent depend on the "touch" of the user,[35] including tuning of the emitter position and other user-tuned source conditions. A comparison of the RMSD values at different emitter positions in the above experiments sheds some light on the origins of this user-dependent "touch" for nESI-IM-MS. Figure 5a shows that variability (as measured by RMSD) for BSA CIU fingerprints collected using a single emitter in each position is higher in the "close" position than in the "far" position. For NIST mAb, CIU fingerprints collected in the close position have a higher RMSD than those collected in the far position when the same emitter is used (Figure 5b). Using a single emitter in a "far" position rather than a "close" position led to more stable spray and a lower (<2%) RMSD value for these ions in most replicates.

However, whereas single-emitter experiments show a clear influence of emitter position on CIU fingerprint repeatability, an assessment of reproducibility using different emitters is more meaningful in characterizing the expected variation of CIU over time within a single lab or between laboratories using the same type of instrument. For the ions studied here, exchanging nESI emitters increased the RMSD by a factor of 1−3 with respect to single-emitter experiments and largely masked any differences in CIU fingerprint variability (RMSD) between the close and far positions (Figure 5). As a caution, it was observed that 1 of 8 emitters tested had an unusually large RMSD of 8.7%, while the others consistently had RMSDs below 4% (analysis with this trial excluded is shown in Figure S15).

Differences in CIU Fingerprints Collected at Different Emitter Positions As Measured by RMSD. In addition to its use as a metric of variability for a single analyte under a single set of experimental conditions, RMSD is also used as a metric to assess structural differences of ions prepared under different experimental conditions or differences between analytes with similar structures. Here, we apply $RMSD_{AofP}$ (average of all pairwise RMSD values between fingerprints in each trial acquired under different experimental conditions) and $RMSD_{PofA}$ (the pairwise RMSD between the average of all trials for each condition, commonly used to assess structural differences between analytes) to assess the differences between fingerprints of the same charge state collected at a close position and a far position. For BSA, the $RMSD_{PofA}$ and $RMSD_{AofP}$ between the fingerprints acquired at the close and far positions are roughly twice those for the data acquired at fixed positions (Figure 5a), indicating a clear effect of the emitter position on CIU behavior for this ion. In contrast, due to the high RMSD between different capillaries in the far position for NIST mAb, it is less clear whether the same effect occurs for this ion (Figure 5b).

Differences in CIU Fingerprints at Different Emitter Positions As Measured Using CIU50. Instead of RMSD, it might seem that the more intuitive property in CIU experiments to compare to the above CID50 results for CID experiments would be CIU50. The BSA and NIST mAb data described above were analyzed using CIUSuite 2 to identify features and CIU50 of transitions for each individual trial (fit parameters are given in Table S2). The results of this analysis are summarized in Figure 6 for both BSA (Figure 6a) and

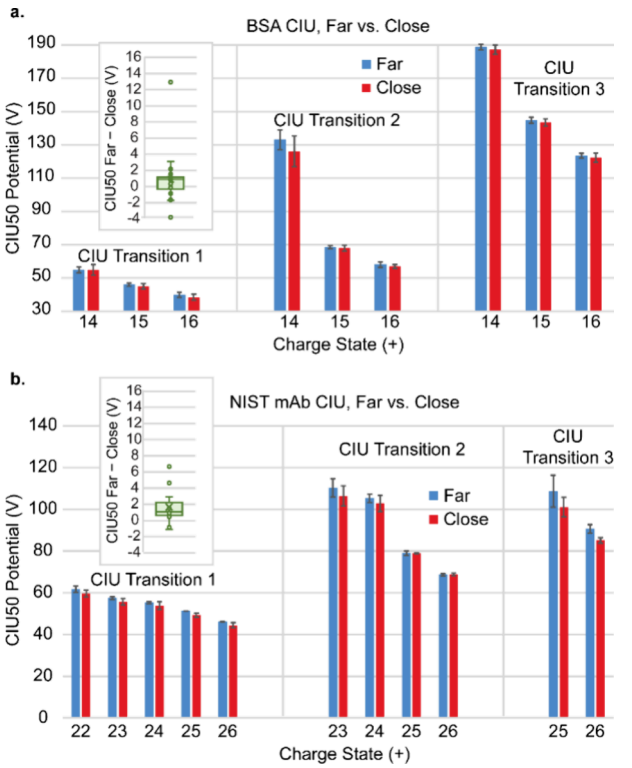

Figure 6. Statistics for CIU50 transitions in far (blue) and close (red) positions for (a) BSA collected on three separate days and (b) NIST mAb collected on a single day. In (a), error bars represent day-to-day variation. In (b), error bars represent variation across the triplicate. Insets show box-and-whisker plots for differences in average CIU50 measured at close and far positions for all charge states and all observed transitions. The unusually high CIU50 difference value in the inset of (a) represents data for one replicate of BSA^{14+} with very low signal.

NIST mAb (Figure 6b). For both NIST mAb and BSA, a small (~2 V average and ~1 V median) shift in CIU50 was observed at a close position. This indicates that the close emitter position causes more in-source activation than the far position, which is in agreement with the CID results. However, the same-day standard deviation in the CIU50 due to exchanging nESI emitters was found to be 1−2 V for these replicates, and the day-to-day standard deviation was ~2 V. Thus, the shift in CIU50 between the two emitter positions was similar in magnitude to the realistic variability of CIU50 caused by exchanging emitters and/or day-to-day instrument drift for the Waters Synapt G2-*Si* instrument.

One explanation for the apparently greater sensitivity of RMSD to emitter position relative to CIU50 is that the latter is determined by integrating IM-MS data over ranges of drift times corresponding to each CIU feature. This integration may average out differences in the shape of drift time distributions

https://doi.org/10.1021/jasms.3c00371
J. Am. Soc. Mass Spectrom. 2024, 35, 498−507

that explicitly increase the RMSD. Thus, RMSD (or other similar metrics that directly account for drift time distribution differences)[65] may be a more sensitive tool than CIU50 for assessing the variability of in-source activation for different experimental conditions when these differences are small. There may also be a kinetic contribution, i.e., the energy barriers for the observed structural transitions for these ions and the internal energy required to observe them on the experimental time scale may differ.

CONCLUSIONS

The data presented here indicate that tuning the emitter position between experiments can be a significant source of day-to-day and emitter-to-emitter differences between CID breakdown curves and CIU fingerprints. However, recording and using identical, micrometer-adjusted nESI emitter positions on a Waters Synapt G2-S*i* instrument can increase the repeatability and reproducibility of CIU/D data. Systematically mapping the emitter-position-dependent shift in CID50 values for holomyoglobin provided a straightforward way to assess which emitter positions led to greater in-source activation, with positions close to the instrument inlet typically exhibiting greater activation (and variability in activation) than far and peripheral positions. In contrast, the emitter position was shown to have a very small influence on CID50 for most analytes on an Agilent 6545XT Q-TOF instrument. This difference between the two instruments likely arises from differences in collisional heating and cooling experienced by the ions as they pass into and through the source regions, which have significantly different pressure profiles and gas dynamics. Modeling this ion heating and cooling as a function of source design, nESI potential, and gas dynamics will be the subject of future investigation.

For CIU fingerprints on the Waters Synapt G2-S*i* instrument, RMSD values indicated that use of close versus far emitter positions can result in measurable differences in BSA CIU fingerprints. CIU50 values, by contrast, were less useful for characterizing emitter position effects due to the high variability in these values when exchanging emitters and due to instrument drift from day to day. For NIST mAb, the RMSD and CIU50 differences between close and far emitter positions were both similar in magnitude to those at a fixed position between emitters and days. These results illustrate that it can be important to characterize emitter position effects on CIU/D for an analyte of interest before choosing which emitter position to use, and that acquiring replicates at a fixed position as well as recording the emitter position can be useful in increasing reproducibility. To support reproducibility and traceability within and between laboratories for native IM-MS experiments, including CIU/D experiments, an example table reporting nESI emitter positions and other relevant experimental settings for these data is included in the SI (see Table S1), and an associated table template is available for download on the Prell group GitHub website (https://github.com/prellgroup).

ASSOCIATED CONTENT

Supporting Information

The Supporting Information is available free of charge at https://pubs.acs.org/doi/10.1021/jasms.3c00371.

Instrument source schematics, SEM measurements of capillary dimensions, ion signal as a function of nESI emitter position, additional CID breakdown curves, representative mass spectra and CIU fingerprints, and a table of nESI emitter properties and instrument settings (PDF)

AUTHOR INFORMATION

Corresponding Author

James S. Prell − *Department of Chemistry and Biochemistry, University of Oregon, Eugene, Oregon 97403-1253, United States; Materials Science Institute, University of Oregon, Eugene, Oregon 97403-1252, United States;* orcid.org/0000-0002-7505-9168; Email: jprell@uoregon.edu

Authors

Samantha O. Shepherd − *Department of Chemistry and Biochemistry, University of Oregon, Eugene, Oregon 97403-1253, United States*

Austin W. Green − *Department of Chemistry and Biochemistry, University of Oregon, Eugene, Oregon 97403-1253, United States*

Elizabeth S. Resendiz − *Department of Chemistry and Biochemistry, University of Oregon, Eugene, Oregon 97403-1253, United States*

Kenneth R. Newton − *Department of Chemistry and Biochemistry, University of Oregon, Eugene, Oregon 97403-1253, United States; Agilent Technologies, Santa Clara, California 95051, United States*

Ruwan T. Kurulugama − *Agilent Technologies, Santa Clara, California 95051, United States*

Complete contact information is available at: https://pubs.acs.org/10.1021/jasms.3c00371

Notes

The authors declare the following competing financial interest(s): The Agilent 6545XT instrument was loaned to the University of Oregon by Agilent Technologies, and this work was supported in part by funding from Agilent Technologies. R.T.K. is an employee of Agilent Technologies.

ACKNOWLEDGMENTS

The authors thank Prof. Joseph Loo for the helpful discussions. This work was supported by funding from the National Institute of General Medical Sciences (Award R01-GM144507 to J.S.P.), the National Science Foundation (Award CHE-1949900 to E.S.R.), and Agilent Technologies (University Relations Award numbers 4732 and 4852). S.O.S. and J.S.P. also thank Agilent Technologies for an instrument loan of the 6545XT and static nESI source.

REFERENCES

(1) Seo, J.; Hoffmann, W.; Warnke, S.; Bowers, M. T.; Pagel, K.; von Helden, G. Retention of Native Protein Structures in the Absence of Solvent: A Coupled Ion Mobility and Spectroscopic Study. *Angew. Chem., Int. Ed.* **2016**, *55* (45), 14173−14176.

(2) Lee, K. W.; Salome, A. Z.; Westphall, M. S.; Grant, T.; Coon, J. J. Onto Grid Purification and 3D Reconstruction of Protein Complexes Using Matrix-Landing Native Mass Spectrometry. *J. Proteome Res.* **2023**, *22* (3), 851−856.

(3) Quintyn, R. S.; Zhou, M.; Yan, J.; Wysocki, V. H. Surface-Induced Dissociation Mass Spectra as a Tool for Distinguishing Different Structural Forms of Gas-Phase Multimeric Protein Complexes. *Anal. Chem.* **2015**, *87* (23), 11879−11886.

(4) Mehmood, S.; Allison, T. M.; Robinson, C. V. Mass Spectrometry of Protein Complexes: From Origins to Applications. *Annu. Rev. Phys. Chem.* **2015**, *66* (1), 453−474.
(5) Rolland, A. D.; Prell, J. S. Computational Insights into Compaction of Gas-Phase Protein and Protein Complex Ions in Native Ion Mobility-Mass Spectrometry. *TrAC Trends Anal. Chem.* **2019**, *116*, 282−291.
(6) Vahidi, S.; Stocks, B. B.; Konermann, L. Partially Disordered Proteins Studied by Ion Mobility-Mass Spectrometry: Implications for the Preservation of Solution Phase Structure in the Gas Phase. *Anal. Chem.* **2013**, *85* (21), 10471−10478.
(7) Bleiholder, C.; Liu, F. C. Structure Relaxation Approximation (SRA) for Elucidation of Protein Structures from Ion Mobility Measurements. *J. Phys. Chem. B* **2019**, *123* (13), 2756−2769.
(8) Vallejo, D. D.; Rojas Ramírez, C.; Parson, K. F.; Han, Y.; Gadkari, V. V.; Ruotolo, B. T. Mass Spectrometry Methods for Measuring Protein Stability. *Chem. Rev.* **2022**, *122* (8), 7690−7719.
(9) Snyder, D. T.; Harvey, S. R.; Wysocki, V. H. Surface-Induced Dissociation Mass Spectrometry as a Structural Biology Tool. *Chem. Rev.* **2022**, *122* (8), 7442−7487.
(10) Rolland, A. D.; Prell, J. S. Approaches to Heterogeneity in Native Mass Spectrometry. *Chem. Rev.* **2022**, *122* (8), 7909−7951.
(11) Rogawski, R.; Sharon, M. Characterizing Endogenous Protein Complexes with Biological Mass Spectrometry. *Chem. Rev.* **2022**, *122* (8), 7386−7414.
(12) Pukala, T.; Robinson, C. V. Introduction: Mass Spectrometry Applications in Structural Biology. *Chem. Rev.* **2022**, *122* (8), 7267−7268.
(13) Bennett, J. L.; Nguyen, G. T. H.; Donald, W. A. Protein-Small Molecule Interactions in Native Mass Spectrometry. *Chem. Rev.* **2022**, *122* (8), 7327−7385.
(14) Keetch, C. A.; Hernández, H.; Sterling, A.; Baumert, M.; Allen, M. H.; Robinson, C. V. Use of a Microchip Device Coupled with Mass Spectrometry for Ligand Screening of a Multi-Protein Target. *Anal. Chem.* **2003**, *75* (18), 4937−4941.
(15) Allison, T. M.; Reading, E.; Liko, I.; Baldwin, A. J.; Laganowsky, A.; Robinson, C. V. Quantifying the Stabilizing Effects of Protein-Ligand Interactions in the Gas Phase. *Nat. Commun.* **2015**, *6* (1), 8551.
(16) Hyung, S.-J.; Robinson, C. V.; Ruotolo, B. T. Gas-Phase Unfolding and Disassembly Reveals Stability Differences in Ligand-Bound Multiprotein Complexes. *Chem. Biol.* **2009**, *16* (4), 382−390.
(17) Zhong, Y.; Han, L.; Ruotolo, B. T. Collisional and Coulombic Unfolding of Gas-Phase Proteins: High Correlation to Their Domain Structures in Solution. *Angew. Chem., Int. Ed.* **2014**, *53* (35), 9209−9212.
(18) Kang, J.; Halseth, T.; Vallejo, D.; Najafabadi, Z. I.; Sen, K. I.; Ford, M.; Ruotolo, B. T.; Schwendeman, A. Assessment of Biosimilarity under Native and Heat-Stressed Conditions: Rituximab, Bevacizumab, and Trastuzumab Originators and Biosimilars. *Anal. Bioanal. Chem.* **2020**, *412* (3), 763−775.
(19) Cong, X.; Liu, Y.; Liu, W.; Liang, X.; Russell, D. H.; Laganowsky, A. Determining Membrane Protein-Lipid Binding Thermodynamics Using Native Mass Spectrometry. *J. Am. Chem. Soc.* **2016**, *138* (13), 4346−4349.
(20) Shirzadeh, M.; Poltash, M. L.; Laganowsky, A.; Russell, D. H. Structural Analysis of the Effect of a Dual-FLAG Tag on Transthyretin. *Biochemistry* **2020**, *59* (9), 1013−1022.
(21) Laganowsky, A.; Reading, E.; Hopper, J. T. S.; Robinson, C. V. Mass Spectrometry of Intact Membrane Protein Complexes. *Nat. Protoc.* **2013**, *8* (4), 639−651.
(22) Laganowsky, A.; Clemmer, D. E.; Russell, D. H. Variable-Temperature Native Mass Spectrometry for Studies of Protein Folding, Stabilities, Assembly, and Molecular Interactions. *Annu. Rev. Biophys.* **2022**, *51* (1), 63−77.
(23) Pacholarz, K. J.; Garlish, R. A.; Taylor, R. J.; Barran, P. E. Mass Spectrometry Based Tools to Investigate Protein-Ligand Interactions for Drug Discovery. *Chem. Soc. Rev.* **2012**, *41* (11), 4335−4355.
(24) Gabelica, V.; Vreuls, C.; Filée, P.; Duval, V.; Joris, B.; Pauw, E. D. Advantages and Drawbacks of Nanospray for Studying Non-covalent Protein-DNA Complexes by Mass Spectrometry. *Rapid Commun. Mass Spectrom.* **2002**, *16* (18), 1723−1728.
(25) Largy, E.; König, A.; Ghosh, A.; Ghosh, D.; Benabou, S.; Rosu, F.; Gabelica, V. Mass Spectrometry of Nucleic Acid Noncovalent Complexes. *Chem. Rev.* **2022**, *122* (8), 7720−7839.
(26) Hammerschmid, D.; van Dyck, J. F.; Sobott, F.; Calabrese, A. N. Interrogating Membrane Protein Structure and Lipid Interactions by Native Mass Spectrometry. In *Biophysics of Membrane Proteins: Methods and Protocols*; Postis, V. L. G., Goldman, A., Eds.; Humana, New York, New York, U.S., 2020; p 233−261. DOI: 10.1007/978-1-0716-0724-4_11.
(27) Sobott, F.; Robinson, C. V. Characterising Electrosprayed Biomolecules Using Tandem-MS—the Noncovalent GroEL Chaperonin Assembly. *Int. J. Mass Spectrom.* **2004**, *236* (1), 25−32.
(28) Kirshenbaum, N.; Michaelevski, I.; Sharon, M. Analyzing Large Protein Complexes by Structural Mass Spectrometry. *J. Vis. Exp.* **2010**, No. 40, 1954.
(29) Wilson, J. W.; Rolland, A. D.; Klausen, G. M.; Prell, J. S. Ion Mobility-Mass Spectrometry Reveals That α-Hemolysin from Staphylococcus Aureus Simultaneously Forms Hexameric and Heptameric Complexes in Detergent Micelle Solutions. *Anal. Chem.* **2019**, *91* (15), 10204−10211.
(30) Perez-Lorenzo, L. J.; Fernandez De La Mora, J. Probing Electrically Driven Nanojets by Energy and Mass Analysis in Vacuo. *J. Fluid Mech.* **2022**, *931*, A4.
(31) Fernández De La Mora, J. The Fluid Dynamics of Taylor Cones. *Annu. Rev. Fluid Mech.* **2007**, *39* (1), 217−243.
(32) Cech, N. B.; Enke, C. G. Practical Implications of Some Recent Studies in Electrospray Ionization Fundamentals. *Mass Spectrom. Rev.* **2001**, *20* (6), 362−387.
(33) Gabelica, V.; De Pauw, E.; Karas, M. Influence of the Capillary Temperature and the Source Pressure on the Internal Energy Distribution of Electrosprayed Ions. *Int. J. Mass Spectrom.* **2004**, *231* (2−3), 189−195.
(34) Benkestock, K.; Sundqvist, G.; Edlund, P.-O.; Roeraade, J. Influence of Droplet Size, Capillary-Cone Distance and Selected Instrumental Parameters for the Analysis of Noncovalent Protein-Ligand Complexes by Nano-Electrospray Ionization Mass Spectrometry. *J. Mass Spectrom.* **2004**, *39* (9), 1059−1067.
(35) Loo, J. A.; Sannes-Lowery, K. A.; Hu, P.; Mack, D. P.; Mei, H.-Y. Studying Noncovalent Protein-RNA Interactions and Drug Binding by Electrospray Ionization Mass Spectrometry. In *New Methods for the Study of Biomolecular Complexes*; Ens, W., Standing, K. G., Chernushevich, I. V., Eds.; Springer, Dordrecht, The Netherlands, 1998; p 83−99. DOI: 10.1007/978-94-015-9046-4_7.
(36) Chen, C. J.; Williams, E. R. The Role of Analyte Concentration in Accelerated Reaction Rates in Evaporating Droplets. *Chem. Sci.* **2023**, *14* (18), 4704−4713.
(37) Oh, M. I.; Consta, S. Stability of a Transient Protein Complex in a Charged Aqueous Droplet with Variable PH. *J. Phys. Chem. Lett.* **2017**, *8* (1), 80−85.
(38) Gadzuk-Shea, M. M.; Hubbard, E. E.; Gozzo, T. A.; Bush, M. F. Sample PH Can Drift during Native Mass Spectrometry Experiments: Results from Ratiometric Fluorescence Imaging. *J. Am. Soc. Mass Spectrom.* **2023**, *34*, 1675.
(39) Chrisman, P. A.; Newton, K. A.; Reid, G. E.; Wells, J. M.; McLuckey, S. A. Loss of Charged versus Neutral Heme from Gaseous Holomyoglobin Ions. *Rapid Commun. Mass Spectrom.* **2001**, *15* (23), 2334−2340.
(40) Van Berkel, G. J.; Asano, K. G.; Schnier, P. D. Electrochemical Processes in a Wire-in-a-Capillary Bulk-Loaded, Nano-Electrospray Emitter. *J. Am. Soc. Mass Spectrom.* **2001**, *12* (7), 853−862.
(41) Brandner, S.; Habeck, T.; Lermyte, F. New Insights into the Intrinsic Electron-Based Dissociation Behavior of Cytochrome c Oligomers. *J. Am. Soc. Mass Spectrom.* **2023**, *34* (9), 1908−1916.

(42) Sterling, H. J.; Cassou, C. A.; Susa, A. C.; Williams, E. R. Electrothermal Supercharging of Proteins in Native Electrospray Ionization. *Anal. Chem.* **2012**, *84* (8), 3795−3801.
(43) Loo, J. A.; Edmonds, C. G.; Udseth, H. R.; Smith, R. D. Collisional Activation and Dissociation of Large Multiply Charged Proteins Produced by Electrospray Ionization. *Anal. Chim. Acta* **1990**, *241* (2), 167−173.
(44) Smith, R. D.; Loa, J. A.; Barinaga, C. J.; Edmonds, C. G.; Udseth, H. R. Collisional Activation and Collision-Activated Dissociation of Large Multiply Charged Polypeptides and Proteins Produced by Electrospray Ionization. *J. Am. Soc. Mass Spectrom.* **1990**, *1* (1), 53−65.
(45) Zhai, H.; Han, X.; Breuker, K.; McLafferty, F. W. Consecutive Ion Activation for Top Down Mass Spectrometry: Improved Protein Sequencing by Nozzle-Skimmer Dissociation. *Anal. Chem.* **2005**, *77* (18), 5777−5784.
(46) Dixit, S. M.; Polasky, D. A.; Ruotolo, B. T. Collision Induced Unfolding of Isolated Proteins in the Gas Phase: Past, Present, and Future. *Curr. Opin. Chem. Biol.* **2018**, *42*, 93−100.
(47) Hopper, J. T. S.; Oldham, N. J. Collision Induced Unfolding of Protein Ions in the Gas Phase Studied by Ion Mobility-Mass Spectrometry: The Effect of Ligand Binding on Conformational Stability. *J. Am. Soc. Mass Spectrom.* **2009**, *20* (10), 1851−1858.
(48) Donor, M. T.; Shepherd, S. O.; Prell, J. S. Rapid Determination of Activation Energies for Gas-Phase Protein Unfolding and Dissociation in a Q-IM-ToF Mass Spectrometer. *J. Am. Soc. Mass Spectrom.* **2020**, *31* (3), 602−610.
(49) Donor, M. T.; Mroz, A. M.; Prell, J. S. Experimental and Theoretical Investigation of Overall Energy Deposition in Surface-Induced Unfolding of Protein Ions. *Chem. Sci.* **2019**, *10* (14), 4097−4106.
(50) Loo, J.; Ogorzalek Loo, R. R. Desolvation of Noncovalently-Bound Complex Ions for ESI-MS Analysis. In *Proceedings of the 43rd ASMS Conference on Mass Spectrometry and Allied Topics*; American Society for Mass Spectrometry, 1995.
(51) Alexander IV, J. N.; Schultz, G. A.; Poli, J. B. Development of a Nano-Electrospray Mass Spectrometry Source for Nanoscale Liquid Chromatography and Sheathless Capillary Electrophoresis. *Rapid Commun. Mass Spectrom.* **1998**, *12* (17), 1187−1191.
(52) Rondeau, D.; Galland, N.; Zins, E.-L.; Pepe, C.; Drahos, L.; Vékey, K. Non-Thermal Internal Energy Distribution of Ions Observed in an Electrospray Source Interfaced with a Sector Mass Spectrometer. *J. Mass Spectrom.* **2011**, *46* (2), 100−111.
(53) Rondeau, D.; Drahos, L.; Vékey, K. Internal Energy Distribution in Electrospray Ionization: Towards the Evaluation of a Thermal-like Distribution from the Multiple-Collision Model. *Rapid Commun. Mass Spectrom.* **2014**, *28* (11), 1273−1284.
(54) Pak, A.; Lesage, D.; Gimbert, Y.; Vékey, K.; Tabet, J.-C. Internal Energy Distribution of Peptides in Electrospray Ionization : ESI and Collision-Induced Dissociation Spectra Calculation. *J. Mass Spectrom.* **2008**, *43* (4), 447−455.
(55) Gabelica, V.; Pauw, E. D. Internal Energy and Fragmentation of Ions Produced in Electrospray Sources. *Mass Spectrom. Rev.* **2005**, *24* (4), 566−587.
(56) Naban-Maillet, J.; Lesage, D.; Bossée, A.; Gimbert, Y.; Sztáray, J.; Vékey, K.; Tabet, J.-C. Internal Energy Distribution in Electrospray Ionization. *J. Mass Spectrom.* **2005**, *40* (1), 1−8.
(57) Iavarone, A. T.; Williams, E. R. Mechanism of Charging and Supercharging Molecules in Electrospray Ionization. *J. Am. Chem. Soc.* **2003**, *125* (8), 2319−2327.
(58) Marty, M. T. Fundamentals: How Do We Calculate Mass, Error, and Uncertainty in Native Mass Spectrometry? *J. Am. Soc. Mass Spectrom.* **2022**, *33* (10), 1807−1812.
(59) Kostelic, M. M.; Hsieh, C.-C.; Sanders, H. M.; Zak, C. K.; Ryan, J. P.; Baker, E. S.; Aspinwall, C. A.; Marty, M. T. Surface Modified Nano-Electrospray Needles Improve Sensitivity for Native Mass Spectrometry. *J. Am. Soc. Mass Spectrom.* **2022**, *33* (6), 1031−1037.
(60) Jordan, J. S.; Xia, Z.; Williams, E. R. Tips on Making Tiny Tips: Secrets to Submicron Nanoelectrospray Emitters. *J. Am. Soc. Mass Spectrom.* **2022**, *33* (3), 607−611.
(61) Gadkari, V. V.; Juliano, B. R.; Mallis, C. S.; May, J. C.; Kurulugama, R. T.; Fjeldsted, J. C.; McLean, J. A.; Russell, D. H.; Ruotolo, B. T. Performance Evaluation of In-Source Ion Activation Hardware for Collision-Induced Unfolding of Proteins and Protein Complexes on a Drift Tube Ion Mobility-Mass Spectrometer. *Analyst* **2023**, *148* (2), 391−401.
(62) Marty, M. T.; Baldwin, A. J.; Marklund, E. G.; Hochberg, G. K. A.; Benesch, J. L. P.; Robinson, C. V. Bayesian Deconvolution of Mass and Ion Mobility Spectra: From Binary Interactions to Polydisperse Ensembles. *Anal. Chem.* **2015**, *87* (8), 4370−4376.
(63) Polasky, D. A.; Dixit, S. M.; Fantin, S. M.; Ruotolo, B. T. CIUSuite 2: Next-Generation Software for the Analysis of Gas-Phase Protein Unfolding Data. *Anal. Chem.* **2019**, *91* (4), 3147−3155.
(64) Gross, D. S.; Zhao, Y.; William, E. R. Dissociation of Heme-Globin Complexes by Blackbody Infrared Radiative Dissociation: Molecular Specificity in the Gas Phase? *J. Am. Soc. Mass Spectrom.* **1997**, *8* (5), 519−524.
(65) Hong, S.; Bush, M. F. Collision-Induced Unfolding Is Sensitive to the Polarity of Proteins and Protein Complexes. *J. Am. Soc. Mass Spectrom.* **2019**, *30* (11), 2430−2437.
(66) Sztáray, J.; Memboeuf, A.; Drahos, L.; Vékey, K. Leucine Enkephalin-A Mass Spectrometry Standard: LEUCINE ENKEPHALIN. *Mass Spectrom. Rev.* **2011**, *30* (2), 298−320.

https://doi.org/10.1021/jasms.3c00371
J. Am. Soc. Mass Spectrom. 2024, 35, 498−507